ORIGINAL ARTICLE

Inhibition of renal fibrosis with a human CXCL9-derived glycosaminoglycan-binding peptide

Fariba Poosti[1], Mohammad Ayodhia Soebadi[2,3], Helena Crijns[1] (iD), Alexandra De Zutter[1] (iD), Mieke Metzemaekers[1], Nele Berghmans[1], Vincent Vanheule[1], Maarten Albersen[2], Ghislain Opdenakker[4], Jo Van Damme[1], Ben Sprangers[1,5], Paul Proost[1†] (iD) & Sofie Struyf[1†] (iD)

[1]Laboratory of Molecular Immunology, Department of Microbiology, Immunology and Transplantation, Rega Institute, KU Leuven, Leuven, Belgium
[2]Laboratory of Experimental Urology, University Hospitals Leuven, Leuven, Belgium
[3]Department of Urology, Faculty of Medicine, Universitas Airlangga, Surabaya, Indonesia
[4]Laboratory of Immunobiology, Department of Microbiology, Immunology and Transplantation, Rega Institute, KU Leuven, Leuven, Belgium
[5]Department of Nephrology, University Hospitals Leuven, Leuven, Belgium

Correspondence

F Poosti or S Struyf, Laboratory of Molecular Immunology, Department of Microbiology, Immunology and Transplantation, Rega Institute, KU Leuven, Herestraat 49-box 1042, 3000, Leuven, Belgium.
E-mails: poosti.fa@gmail.com or sofie.struyf@kuleuven.be

†Equal contributors.

Abstract

Objectives. Renal fibrosis accompanies all chronic kidney disorders, ultimately leading to end-stage kidney disease and the need for dialysis or even renal replacement. As such, renal fibrosis poses a major threat to global health and the search for effective therapeutic strategies to prevent or treat fibrosis is highly needed. We evaluated the applicability of a highly positively charged human peptide derived from the COOH-terminal domain of the chemokine CXCL9, namely CXCL9(74–103), for therapeutic intervention. Because of its high density of net positive charges at physiological pH, CXCL9(74–103) competes with full-length chemokines for glycosaminoglycan (GAG) binding. Consequently, CXCL9(74–103) prevents recruitment of inflammatory leucocytes to sites of inflammation. **Methods.** CXCL9(74–103) was chemically synthesised and tested *in vitro* for anti-fibrotic properties on human fibroblasts and *in vivo* in the unilateral ureteral obstruction (UUO) mouse model. **Results.** CXCL9(74–103) significantly reduced the mRNA and/or protein expression of connective tissue growth factor (CTGF), alpha-smooth muscle actin (α-SMA) and collagen III by transforming growth factor (TGF)-β1-stimulated human fibroblasts. In addition, administration of CXCL9(74–103) inhibited fibroblast migration towards platelet-derived growth factor (PDGF), without affecting cell viability. In the UUO model, CXCL9(74–103) treatment significantly decreased renal α-SMA, vimentin, and fibronectin mRNA and protein expression. Compared with vehicle, CXCL9(74–103) attenuated mRNA expression of TGF-β1 and the inflammatory markers/mediators MMP-9, F4/80, CCL2, IL-6 and TNF-α. Finally, CXCL9(74–103) treatment resulted in reduced influx of leucocytes in the UUO model and preserved tubular morphology. The anti-fibrotic and anti-inflammatory effects of CXCL9(74–103) were mediated by competition with chemokines

and growth factors for GAG binding. **Conclusions.** Our findings provide a scientific rationale for targeting GAG–protein interactions in renal fibrotic disease.

INTRODUCTION

Renal fibrosis provokes the excessive deposition of extracellular matrix resulting in kidney dysfunction. It is consistently associated with chronic kidney disease (CKD), leading to end-stage kidney disease (ESKD) and demanding renal replacement therapy.[1] Therefore, new therapies that halt fibrogenesis and the subsequent progression to ESKD are urgently needed. Persistent inflammation has appeared to be a key driver of fibrosis progression in both diabetic and non-diabetic kidney diseases.[2] Supporting this notion is the fact that high levels of inflammatory markers in blood or urine usually reflect a high risk of developing functional kidney decline. This indicates that chronic non-resolving inflammation probably has a central role in the development of renal fibrosis.[3]

Inflammation involves the accumulation and activation of leucocytes driven by designated guidance molecules known as chemokines. Within tissues, different cell types such as resident leucocytes, fibroblasts and endothelial cells are capable of secreting chemokines. Chemokines exert their biological functions by activating dedicated seven-transmembrane G protein-coupled receptors (GPCRs).[4–7] However, additional interaction partners, in particular glycosaminoglycans (GAGs), are critically implicated in regulating chemokine function and availability *in vivo*.[8,9] Moreover, the function of chemokines and their receptors is regulated by post-translational modifications.[10]

Besides regulating the influx of immune cells at sites of injury, additional functions for chemokines in tissue fibrosis have been recently uncovered.[11,12] For instance, C-X-C chemokine ligand 9 (CXCL9), a member of the CXC chemokine family that binds to CXC chemokine receptor 3 (CXCR3), not only directs activation, migration and differentiation of immune cells,[13–15] but also modulates angiogenesis and epithelial-to-mesenchymal transition (EMT) and reduces fibrosis in carbon tetrachloride-treated mice.[16,17] Moreover, the inhibition of pulmonary fibrosis by the CXCR3-activating chemokine CXCL10 was shown to be dependent on its GAG-binding properties.[18] Furthermore, polymorphisms affecting the three interferon (IFN)-γ-inducible CXCR3 ligands CXCL9, CXCL10 and CXCL11 were associated with liver fibrosis.[19] In addition, the absence of CXCR3 led to progressive lung fibrosis in the bleomycin-induced lung injury model.[20]

Similar to other CXCR3 ligands, the production of CXCL9 is induced by the Th1 cytokine IFN-γ. The secreted human CXCL9 protein consists of 103 amino acids and is characterised by a remarkably long, positively charged COOH-terminus, which is absent in most other chemokines.[13] The COOH-terminal region of CXCL9 contains GAG-binding motifs that are physically separated from its CXCR3 interaction domain. COOH-terminally truncated CXCL9 proteins were identified to be produced by several cell types, such as human fibroblasts and leucocytes.[21,22] Because of the high number of positive charges, some COOH-terminal human CXCL9 peptides can bind to GAGs with higher affinity than most intact chemokines. As such, they exert anti-inflammatory effects by competing with intact chemokines for GAG binding, thereby inhibiting neutrophil extravasation.[22] In previous studies, we showed that the synthetic CXCL9(74–103) peptide competed with CXCL8 for binding to GAGs and inhibited neutrophil migration *in vivo* in monosodium urate crystal-induced gout, antigen-induced arthritis and dinitrofluorobenzene-induced contact hypersensitivity.[22–25] Moreover, as a result of competition for viral attachment to GAGs, the peptide possesses antiviral properties against herpes simplex virus, dengue virus and respiratory syncytial virus.[26] However, the effect of this peptide on fibrosis was unknown. In the present study, the potential therapeutic properties of CXCL9(74–103) were evaluated *in vitro,* in fibroblast cultures, and *in vivo,* in the unilateral ureteral obstruction (UUO) mouse model for renal fibrosis.

RESULTS

Full-length CXCL9 shows anti-fibrotic effects on TGF-β1-stimulated human fibroblasts

The anti-fibrotic role of full-length human CXCL9 has been reported in animal models of fibrosis.[16,27] We confirmed the anti-fibrotic potential of the intact chemokine *in vitro* by stimulating primary human fibroblasts with 5 ng mL^{-1} of TGF-β1 in the presence of full-length CXCL9(1–103). The intact chemokine significantly reduced α-SMA mRNA expression at concentrations of 1–100 nM (Figure 1a). However, a significant reduction in collagen III mRNA expression was observed only at the highest test concentration (100 nM) of CXCL9(1–103) (Figure 1b). These data indicate that CXCL9(1–103) counteracts the pro-fibrotic properties of TGF-β1 on human fibroblasts.

Synthesis and functional characterisation of human CXCL9-derived peptides

A highly cationic COOH-terminal peptide of human CXCL9, that is CXCL9(74–103), and the NH$_2$-terminal chemokine domain, CXCL9(1–78), were chemically synthesised, deprotected and purified by RP-HPLC to investigate their effects on fibrosis (Figure 2a). Part of the synthesised CXCL9(74–103) was fluorescently labelled with TAMRA at the NH$_2$-terminus to study the *in vivo* biodistribution of the peptide. The correct relative molecular masses (Mr) of the synthetic peptides were confirmed by ion trap mass spectrometry (Figure 2b). A ball-and-stick model of the structure of CXCL9(1–103) is shown in Figure 2c, with the GAG-binding region indicated in pink and green.

The two synthesised peptides displayed highly different capacities to activate signal transduction downstream of CXCR3. Whereas the COOH-terminal peptide CXCL9(74–103) failed to provoke calcium-dependent signalling in CXCR3-transfected CHO cells, CXCL9(1–78) induced a clear increase in intracellular calcium levels [48.4 nM ± 2.8 ($n = 6$)] albeit with lower efficiency compared with intact CXCL9 [calcium response of 598.1 ± 22.9 nM ($n = 4$)].[28]
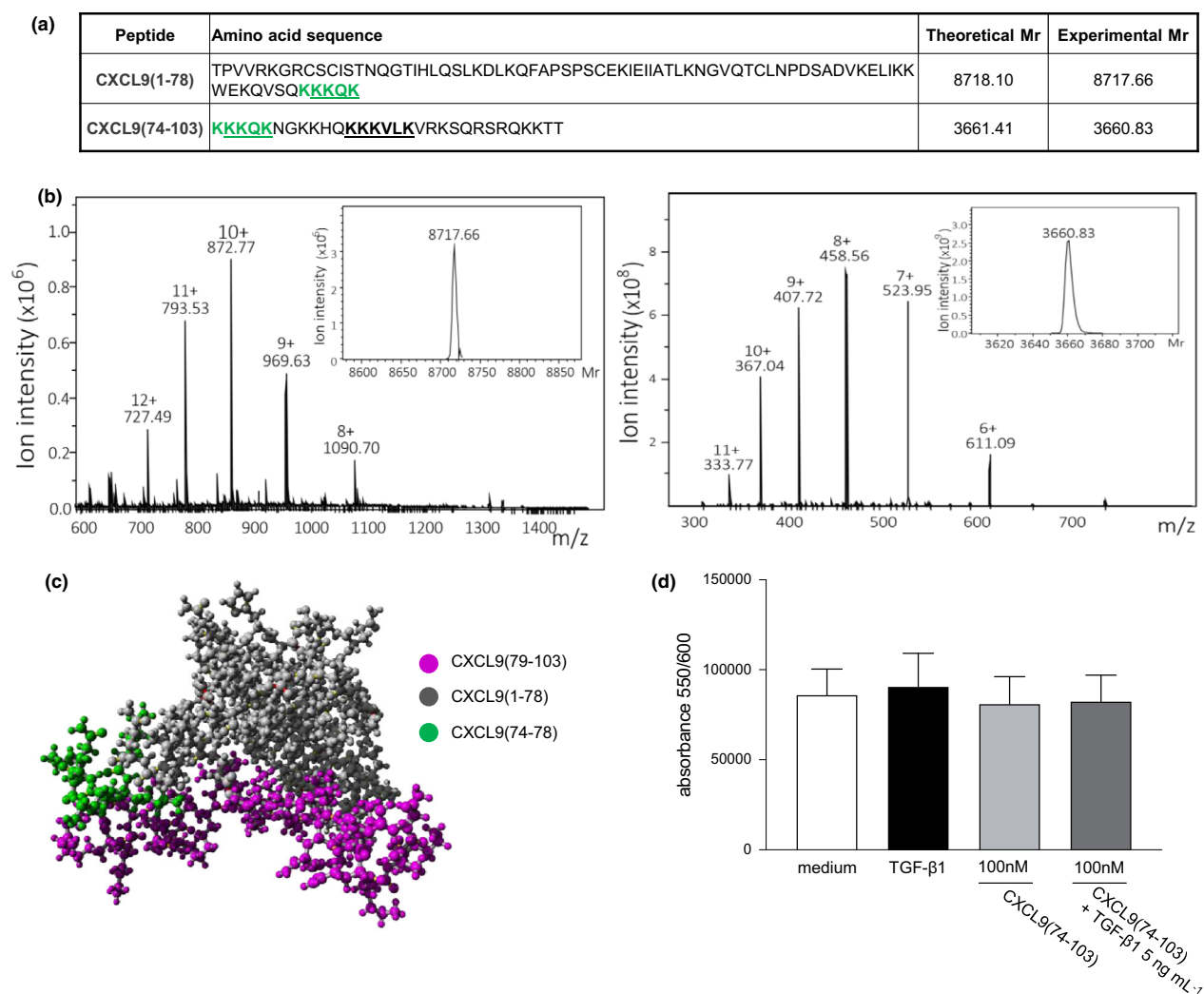
Effect of CXCL9(74–103) on fibroblast viability

Before evaluating the putative anti-fibrotic potential of CXCL9(74–103) on human fibroblasts, we first determined whether the peptide exerted adverse effects on cell viability using the non-toxic, cell-permeable redox indicator alamarBlue. Incubation with the peptide alone or in the presence of TGF-β1 did not reveal any cytotoxic effects as the conversion of the dye was similar in all conditions tested (Figure 2d).

CXCL9(74–103) competes with TGF-β1 for binding to heparan sulphate

Transforming growth factor-β1 (TGF-β1) is a major pro-fibrotic cytokine that plays a crucial role in
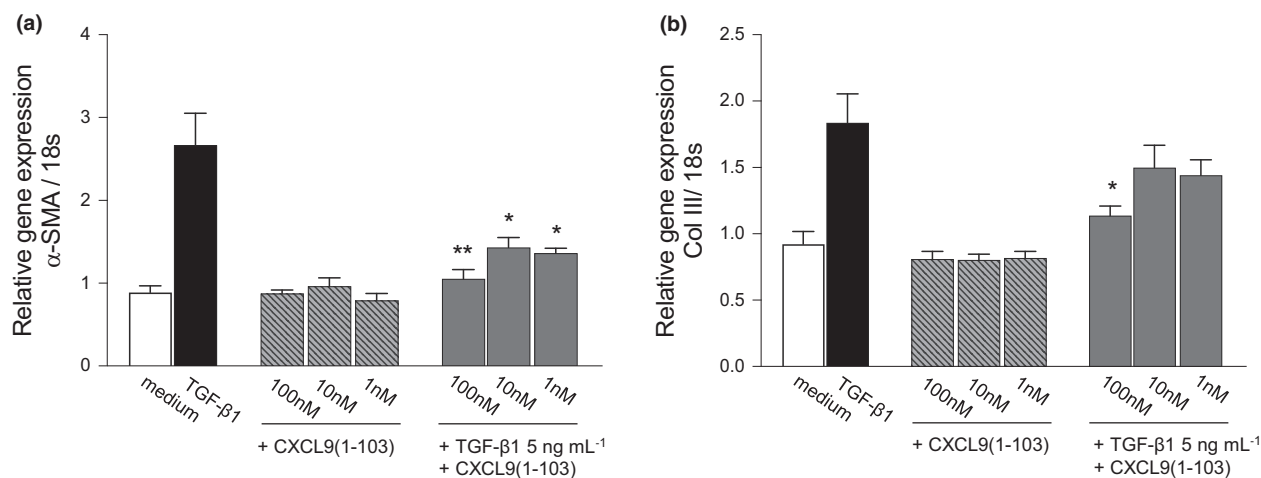
Figure 1. *In vitro* anti-fibrotic effect of intact CXCL9. Human primary fibroblasts were seeded in 6-well plates and incubated with medium alone (control), intact CXCL9 (1 to 100 nM), TGF-β1 alone (5 ng mL^{-1}) or TGF-β1 (5 ng mL^{-1}) in combination with CXCL9 (1 to 100 nM). Relative mRNA expression of the fibrotic markers **(a)** α-SMA and **(b)** collagen III is shown and reported as mean ± SEM ($n = 4$; the four independent experiments were performed in duplicate, and each cDNA sample was analysed twice). *$P < 0.05$, **$P < 0.01$ versus TGF-β1.

(a)

Peptide	Amino acid sequence	Theoretical Mr	Experimental Mr
CXCL9(1-78)	TPVVRKGRCSCISTNQGTIHLQSLKDLKQFAPSPSCEKIEIIATLKNGVQTCLNPDSADVKELIKKWEKQVSQ**KKKQK**	8718.10	8717.66
CXCL9(74-103)	**KKKQK**NGKKHQ**KKKVLK**VRKSQRSRQKKTT	3661.41	3660.83

(b)

(c)

- CXCL9(79-103)
- CXCL9(1-78)
- CXCL9(74-78)

(d)

Figure 2. Overview of the synthesised CXCL9 isoforms and effect of CXCL9(74–103) on cell viability. **(a)** Amino acid sequence and theoretical and experimentally determined relative molecular masses (Mr) of CXCL9(1–78) and CXCL9(74–103). The GAG-binding motifs are underlined. The residues present in the synthesised NH$_2$-terminal chemokine domain and the COOH-terminal GAG-binding peptide are indicated in green. **(b)** The CXCL9-derived peptides were chemically synthesised based on Fmoc chemistry, and their quality was evaluated by mass spectrometry. The intensities of the detected ions in function of their specific mass/charge (*m/z*) ratio are shown for folded CXCL9(1–78) and CXCL9(74–103). To calculate the Mr of the peptides from the charged ions, Bruker deconvolution software was used. The experimentally determined Mr of the peptides is shown as an insert on the upper right of the average unprocessed mass spectra. **(c)** Ball-and-stick model structure of full-length CXCL9(1–103). The residues present in the synthesised NH$_2$-terminal chemokine domain and COOH-terminal GAG-binding peptide are indicated in green. **(d)** Human primary fibroblasts were cultured in a 96-well plate and incubated with CXCL9(74–103) alone or in the presence of TGF-β1 (5 ng mL^{-1}). Cell viability was measured after 48 h using the alamarBlue assay. Error bars indicate the SEM for $n = 4$ experiments. In each experiment, all conditions were tested in duplicate.

fibroblast activation and production, and in remodelling of the extracellular matrix.[29,30] TGF-β1 is known to interact with heparin and heparan sulphate (HS), which enhances its activity and prevents proteolytic degradation.[31–34] Therefore, we used an ELISA-like GAG-binding competition assay to determine whether the CXCL9-derived peptides competed with TGF-β1 for binding to HS.

Interestingly, a dose-dependent, negative effect of CXCL9(74–103) on TGF-β1–HS complex formation was found. As expected, the NH$_2$-terminal chemokine domain CXCL9(1–78) – bearing only one GAG-binding domain and lacking a number of additional positively charged amino acids – failed to interrupt TGF-β1–HS interaction (Figure 3a). These results collectively suggest that CXCL9(74–103), with

its two GAG-binding motifs, attenuates TGF-β1–HS binding and might consequently block the pro-fibrotic properties of TGF-β1.

In vitro anti-fibrotic effects of CXCL9-derived peptides

Given the anti-inflammatory effects of CXCL9-derived peptides observed in our previous studies, and their ability to modulate the binding of TGF-β1 to HS, we next investigated the putative anti-fibrotic effects of CXCL9(74–103) on fibroblast activation in vitro, by evaluating interference of the peptide with platelet-derived growth factor (PDGF) and TGF-β1 activity.

PDGF, being capable of inducing mesenchymal cell proliferation, migration and extracellular matrix deposition, is one of the central mediators involved in fibrosis.[35] We investigated the effect of CXCL9(74–103) on PDGF-induced migration of fibroblasts. Human diploid fibroblasts were incubated with PDGF (30 ng mL^{-1}) to induce migration. CXCL9(74–103) at 3 μM significantly reduced the PDGF-induced migratory response of human fibroblasts (Figure 3b).

Connective tissue growth factor, a downstream mediator of TGF-β1, modulates myofibroblast activation and is associated with multiple fibrotic disorders.[36] We examined the effect of the peptide on the production of CTGF by fibroblasts after treatment with TGF-β1. Human diploid fibroblasts were incubated with TGF-β1 (5 ng mL^{-1}) in the presence or absence of CXCL9(74–103). CXCL9(74–103) at 100 nM caused a
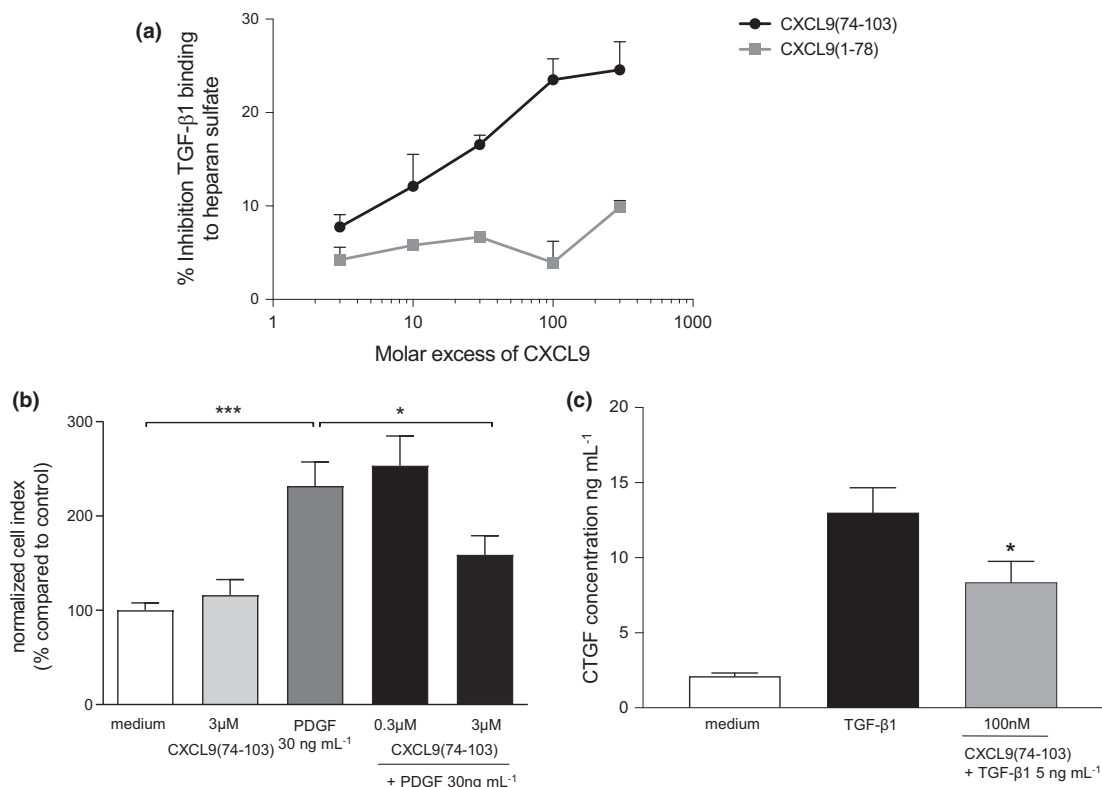
Figure 3. Effect of CXCL9(74–103) on TGF-β1 and PDGF. **(a)** Competition of recombinant human TGF-β1 with CXCL9(1–78) or CXCL9(74–103) for binding to heparan sulphate-coated plates was tested. Results are expressed as the percentage inhibition of TGF-β1 binding to heparan sulphate and shown as mean ± SEM ($n = 2$). **(b)** The xCELLigence Real-Time Cell Analyzer was used to measure fibroblast migration. PDGF-β (30 ng mL^{-1}) or medium (control) was added to the wells of the lower chamber, and medium with or without CXCL9(74–103) (0.3 or 3 μM) was added with the fibroblasts in the upper chamber. In each experiment, all conditions were tested at least in duplicate. Data represent mean ± SEM ($n = 3$). *$P < 0.05$, ***$P < 0.001$ versus PDGF. **(c)** To determine the effect of CXCL9(74–103) on TGF-β1-induced CTGF production, fibroblasts were seeded in six-well plates and either left untreated or stimulated with TGF-β1 in the presence or absence of 100 nM of CXCL9(74–103). After 48 h, an enzyme-linked immunosorbent sandwich assay (ELISA) was used to measure CTGF production ($n = 5$; conditions were tested in duplicate in each experiment). *$P < 0.05$.

significant decrease in the production of CTGF (Figure 3c).

We also evaluated changes in fibroblast activation (based on α-SMA expression) and production of the extracellular matrix protein collagen III upon treatment with TGF-β1 (5 ng mL^{-1}) in the presence or absence of CXCL9(74–103) (1–100 nM). We observed that, in contrast to TGF-β1, the peptide alone did not affect the expression of the fibrotic genes α-SMA and collagen III (Figure 4). However, the GAG-binding peptide CXCL9(74–103) markedly reduced α-SMA and collagen III mRNA expression induced by TGF-β1 (5 ng mL^{-1}; Figure 4a and b). Also, α-SMA and collagen III protein levels were reduced upon administration of CXCL9(74–103) (Figure 4c and d). Representative photomicrographs of α-SMA and collagen III staining are shown in Figure 4e.

In vivo biodistribution of TAMRA-labelled CXCL9(74–103) in a mouse model of renal fibrosis

Before evaluating the *in vivo* effect of CXCL9(74–103) on fibrosis, we assessed the biodistribution of the peptide in the UUO mouse model. After the UUO procedure, osmotic pumps were subcutaneously implanted to deliver TAMRA-labelled CXCL9(74–103) over 7 days. The presence of the TAMRA fluorescence in different organs was determined on day 7 and day 10 after implantation of the pumps. As shown in Figure 5a, the highest fluorescence signal was observed in the kidneys, and a rather similar signal was measured in the UUO and contralateral kidney 10 days after implantation. Notably, other organs from these mice (heart, lung, liver and spleen) and plasma displayed at least ten times lower but consistent levels of TAMRA fluorescence on days 7 and 10 (Figure 5b).

CXCL9(74–103) reduces α-SMA and vimentin expression in the UUO mouse model of renal fibrosis

To investigate whether CXCL9(74–103) treatment attenuated fibrosis, expression levels of fibroblast activation markers (α-SMA and vimentin) were determined in vehicle- versus CXCL9(74–103)-treated UUO kidneys. UUO induced an increase in α-SMA and vimentin mRNA expression 7 days after surgery, which was significantly reduced by

CXCL9(74–103) in a dose-dependent manner (Figure 6a and b).

We next analysed whether the CXCL9(74–103)-induced reduction in α-SMA and vimentin mRNA expression also translated into diminished levels of the encoded proteins by immunofluorescence microscopy. UUO caused a significant increase in interstitial α-SMA and vimentin protein abundance 7 days post-surgery. CXCL9(74–103) treatment significantly lowered UUO-induced α-SMA and vimentin protein levels (Figure 6c and d). Representative photomicrographs of α-SMA and vimentin staining of UUO kidneys are shown in Figure 6e. These data collectively indicate that CXCL9(74–103) effectively reduces fibroblast activation induced by UUO.

CXCL9(74–103) treatment reduces extracellular matrix production in the UUO model

Next, we studied the effect of CXCL9(74–103) on extracellular matrix deposition by analysing fibronectin and collagen III expression (Figure 7). UUO induced a prominent increase in fibronectin (Figure 7a) and collagen III (Figure 7b) mRNA and protein expression (Figure 7c and d) at day 7 post-UUO. Treatment with 4 mg mL^{-1} CXCL9(74–103) significantly reduced UUO-induced fibronectin expression both on the mRNA and on the protein level (Figure 7a and c). Compared with vehicle-treated kidneys, a trend towards reduced collagen III expression was observed in kidneys treated with 4 mg mL^{-1} CXCL9(74–103) (Figure 7b and d). Representative photomicrographs of fibronectin and collagen III staining are shown in Figure 7e.

CXCL9(74–103) reduces mRNA expression of MMP-9 and TGF-β1

Matrix metalloproteinase-9 (MMP-9) has been shown to activate latent TGF-β,[37,38] suggesting a pro-fibrotic role for MMP-9. Hence, we evaluated the effect of the CXCL9-derived peptide on MMP-9 expression. UUO significantly increased MMP-9 mRNA expression. Treatment of mice with 0.4 or 4 mg mL^{-1} CXCL9(74–103) significantly attenuated the UUO-induced enhancement of MMP-9 mRNA expression 7 days after surgery (Figure 8a). In addition, TGF-β1 mRNA expression, upregulated by the UUO procedure, was reduced in CXCL9(74–103)-treated mice (Figure 8b).
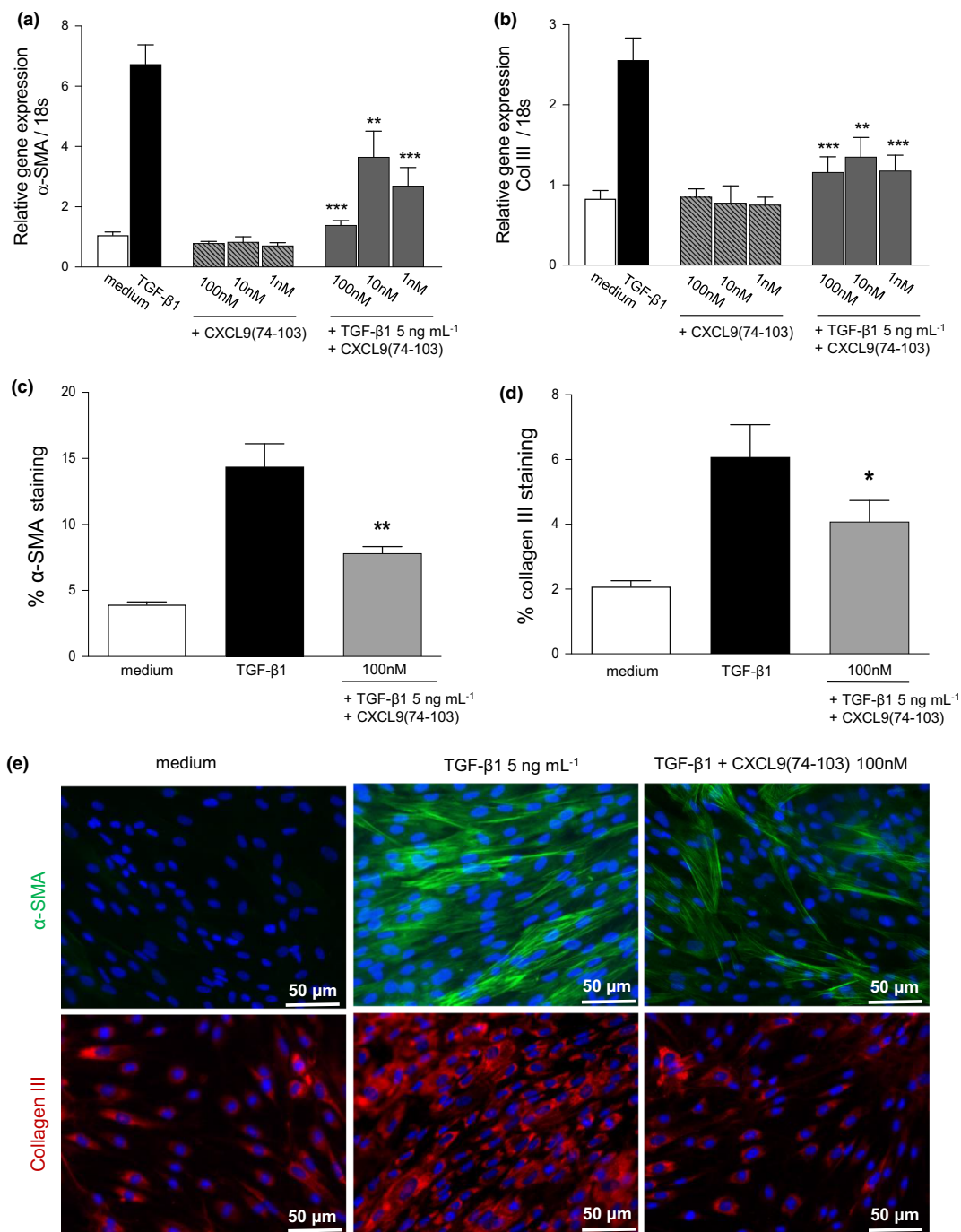
Figure 4. *In vitro* anti-fibrotic effect of CXCL9(74–103). Relative mRNA expression of **(a)** α-SMA and **(b)** collagen III in human diploid fibroblasts incubated with medium alone (control), TGF-β1 (5 ng mL^{-1}), CXCL9(74–103) (1–100 nM) or TGF-β1 (5 ng mL^{-1}) in combination with CXCL9 (74–103). Quantitative analysis of **(c)** α-SMA and **(d)** collagen III protein expression as determined by immunocytochemistry. **(e)** Representative images of cells treated with medium, TGF-β1 alone or in combination with CXCL9(74–103), stained with antibodies against collagen III or α-SMA. Data are presented **(a–d)** as mean ± SEM (*n* = 4; conditions were tested in duplicate in each experiment, and each sample was analysed twice). *$P < 0.05$, **$P < 0.01$, ***$P < 0.001$ versus TGF-β1.
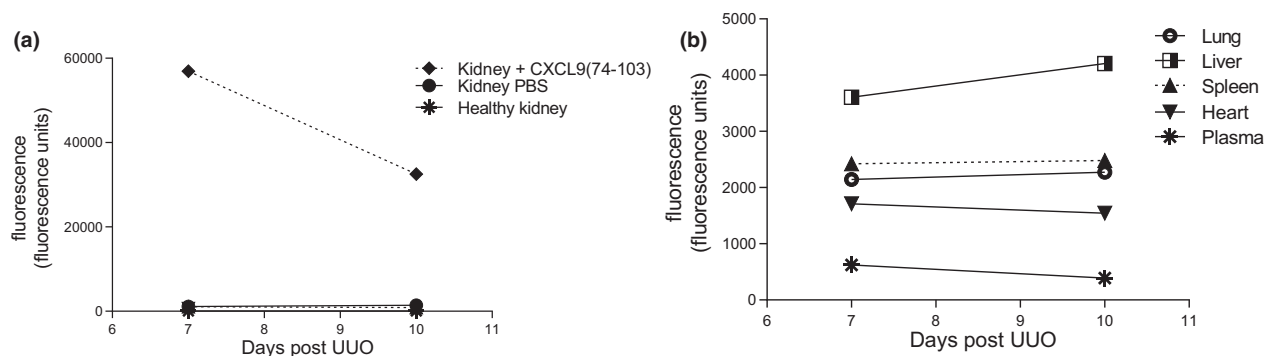
Figure 5. *In vivo* biodistribution of TAMRA-labelled CXCL9(74–103) in the kidney fibrosis model (UUO). Mice (*n* = 4 mice per group) were subjected to UUO of the left kidney, and subsequently, osmotic pumps were implanted subcutaneously. On day 7 or 10 after surgery, mice were euthanized. Blood and organs were collected, and the fluorescence intensity was measured. **(a)** CXCL9(74–103) biodistribution was evaluated as the amount of TAMRA-labelled peptide fluorescence in UUO kidneys compared to healthy kidneys and kidneys of mice injected with vehicle. **(b)** Fluorescent peptide biodistribution in plasma and indicated organs (excitation, 535–20 nm and emission, 585–30 nm). Notice the difference in the range of the *y*-axis in the two panels.

CXCL9(74–103) preserves tubular morphology

Unilateral ureteral obstruction evokes substantial changes in normal kidney morphology. We thus sought to determine whether the CXCL9(74–103)-induced attenuation of renal fibrosis was accompanied by preservation of tubular morphology. The cortical tubular luminal area was measured in UUO-vehicle-treated kidneys versus UUO-CXCL9(74–103)-treated kidneys. In UUO kidneys, the mean tubular luminal areas increased significantly in comparison with those of healthy control kidneys (data not shown), indicating tubular dilation. CXCL9(74–103)-treated UUO kidneys had a significant attenuation of tubular dilation (Figure 8c and d).

CXCL9(74–103) attenuates inflammation in the UUO mouse model of renal fibrosis

Since inflammation is an essential trigger for fibrosis, we evaluated whether the upregulation of inflammatory markers in UUO was influenced by CXCL9(74–103) treatment. The qRT-PCR analysis revealed increased mRNA levels of F4/80, CCL2, TNF-α and IL-6 in UUO kidneys 7 days after induction of the disease. Mice that received 4 mg mL^{-1} of CXCL9(74–103) showed a significant reduction in the mRNA expression of these inflammatory markers (Figure 9a–d). At a 10-fold lower dose, CXCL9(74–103) significantly decreased IL-6 mRNA expression levels but failed to significantly reduce the expression of the other markers of inflammation. We also performed flow cytometry to analyse cell infiltration in response to ureter ligation. The percentage of leucocytes (CD45$^+$) in the UUO kidney was moderately reduced in the CXCL9(74–103)-treated mice (Figure 9e). This decrease was primarily caused by impaired recruitment of monocytes (F4/80$^+$) as their percentage significantly decreased (Figure 9f). This could be the consequence of both a lower production of the monocyte-attracting chemokine CCL2 (Figure 9d) and a less efficient chemokine presentation on renal vessels. The percentages of neutrophils (Figure 9g) and lymphocytes (results not shown) were not significantly altered, though absolute counts of these cell types tended to be lower.

DISCUSSION

Chemokines are professional guidance proteins orchestrating the directional migration of specific leucocyte subsets during homeostasis and in inflammation.[39] Over the past few decades, it gradually became clear that chemokines can be critically involved in numerous other physiological and pathological processes including fibrosis.[16–19,40–42] For instance, the chemokine receptor CXCR3 and its IFN-γ-inducible ligands, that is CXCL9 to CXCL11, are not only important for the attraction of activated T cells and natural killer cells but also influence fibrosis.[14–20] The
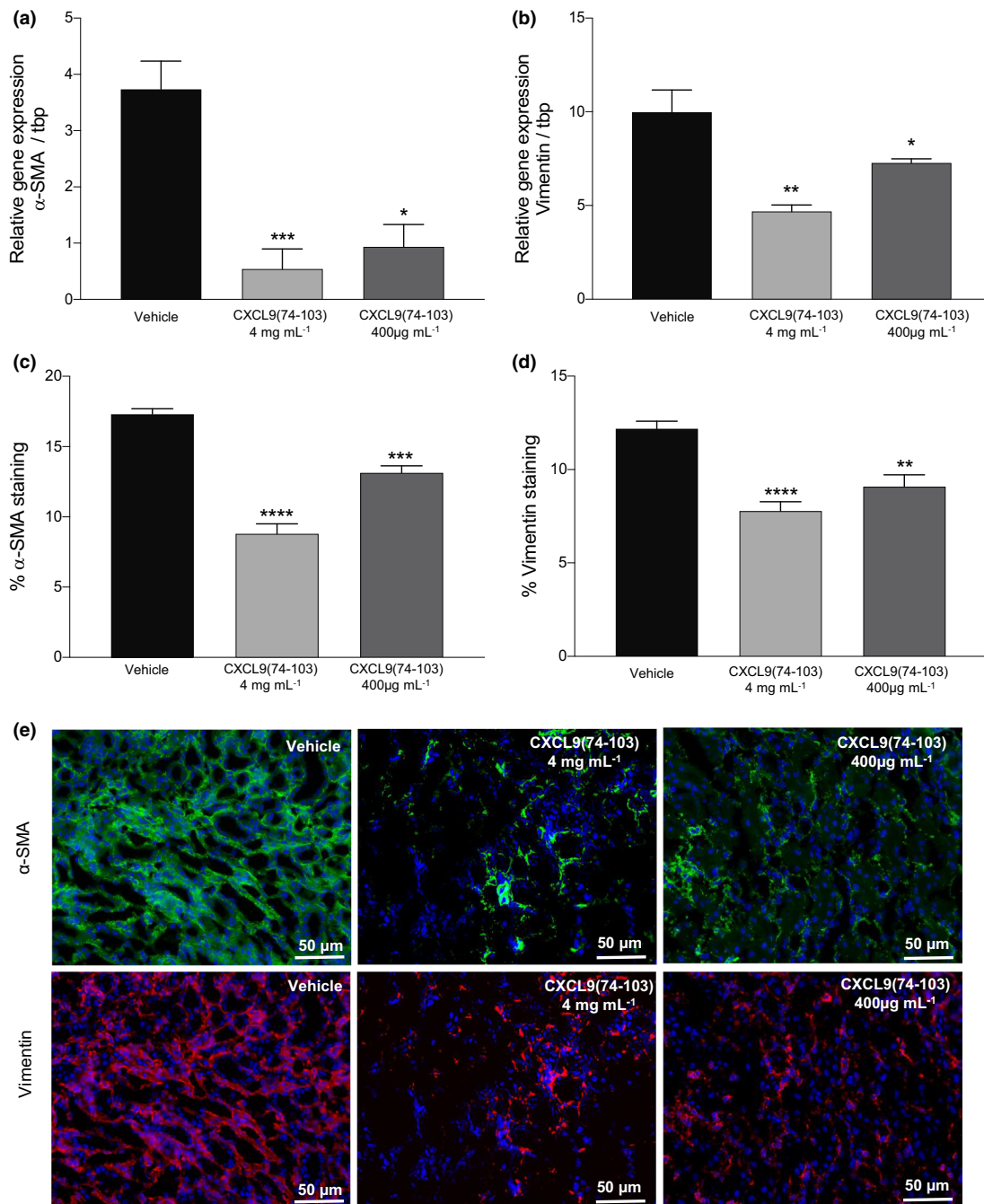
Figure 6. Inhibition of α-SMA and vimentin expression by CXCL9(74–103). Osmotic pumps containing 0.4 or 4 mg mL^{-1} of CXCL9(74–103) peptide (100 μL per pump) were implanted in mice shortly after UUO surgery. Relative gene expression of **(a)** α-SMA and **(b)** vimentin in UUO kidneys at day 7 post-surgery. Quantitative analysis at day 7 post-surgery of **(c)** α-SMA and **(d)** vimentin protein expression. **(e)** Photomicrographs (scale bars are 50 μm) of α-SMA and vimentin immunohistochemical analysis (evaluated at 200× magnification). Data are presented **(a–d)** as mean ± SEM of 6 mice per group. Each cDNA sample was analysed in duplicate. Staining was quantified in 5 microscopic fields per kidney. *$P < 0.05$, **$P < 0.01$, ***$P < 0.001$, ****$P < 0.0001$ versus vehicle.

potentially pathological functions fulfilled by distinct chemokines provide a scientific *rationale* for targeting these proteins in human disease.

Strikingly, the majority of mouse CXC chemokine genes are colocalised within a chromosomal region that contains fibrogenic genes.[43]
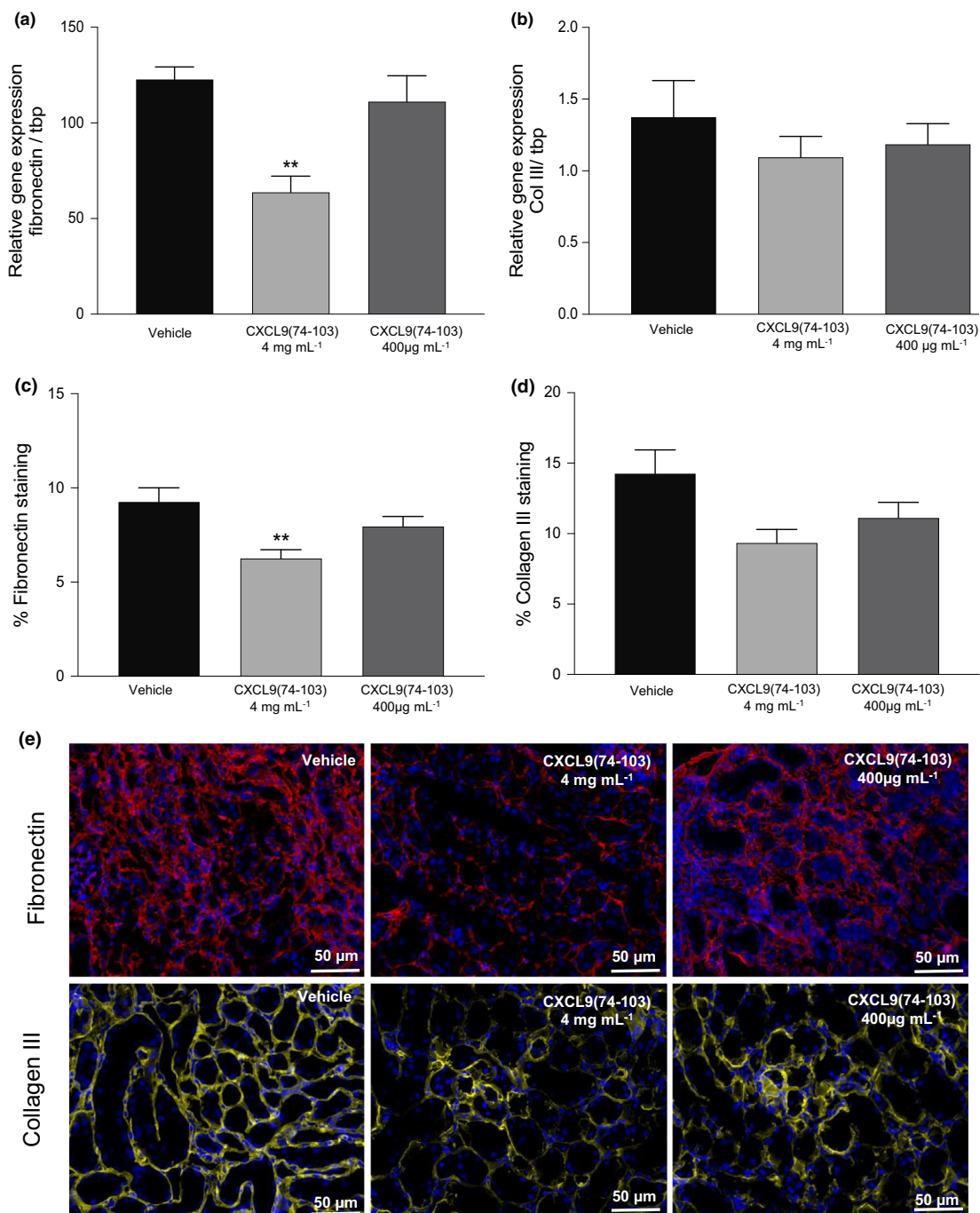
Figure 7. Effect of CXCL9(74–103) on extracellular matrix deposition. Relative gene expression of **(a)** fibronectin and **(b)** collagen III in UUO kidneys at day 7 post-surgery. Computerised quantitative analysis at day 7 post-surgery of **(c)** fibronectin and **(d)** collagen III protein expression. **(e)** Photomicrographs (scale bars are 50 μm) of fibronectin and collagen III immunohistochemical analysis (evaluated at 200× magnification). Data are presented **(a–d)** as mean ± SEM of six mice per group. Each cDNA sample was analysed in duplicate. Staining was quantified in five microscopic fields per kidney. **$P < 0.01$ versus vehicle.

Multiple approaches to tackling chemokine-driven biological processes have come into view. Because of the key role played by GAGs in the regulation of chemokine activity and availability, one approach may be to create chemokine derivatives with superior GAG-binding properties that fail to activate GPCRs.[44–47] Such peptides, by competing with full-length, active chemokines for
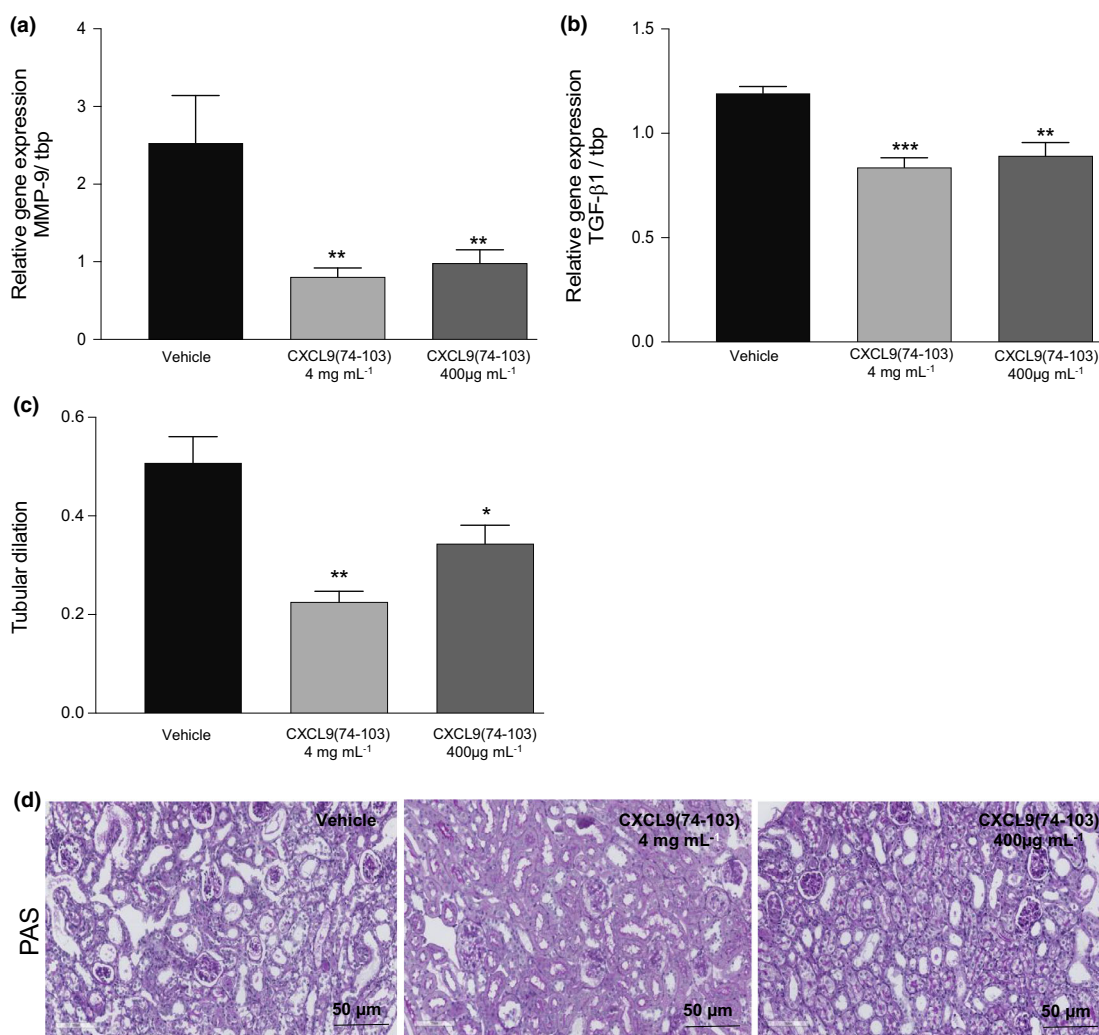
Figure 8. Effect of CXCL9(74–103) on MMP-9 and TGF-β1 expression and tubular dilation in UUO mice. The relative gene expression of **(a)** MMP-9 and **(b)** TGF-β1 was evaluated in UUO kidneys 7 days post-surgery. **(c)** Computerised quantitative analysis of tubular dilation, which was quantified as the ratio of surface area tubular lumen/surface area tubular lumen + epithelium in UUO mice treated with vehicle (PBS), 0.4 mg mL^{-1} or 4 mg mL^{-1} of CXCL9(74–103) (7 days post-surgery). Data are presented **(a–c)** as mean ± SEM of six mice per group. Each cDNA sample was analysed in duplicate. Five randomly selected microscopic fields per kidney were analysed *P < 0.05, **P < 0.01, ***P < 0.001 versus vehicle. **(d)** Representative photomicrographs of PAS-stained kidney (scale bars are 50 μm) sections of UUO mice treated with vehicle (PBS), 0.4 mg mL^{-1} or 4 mg mL^{-1} of CXCL9(74–103) (7 days post-surgery) (200×).

GAG binding, reduce the local concentration of intact chemokines to prevent the formation of a chemotactic gradient and render chemokines more sensitive to proteolytic degradation.[28,48] Recently, we showed that a peptide derived from the COOH-terminal domain of human CXCL9, that is CXCL9(74–103), meets these criteria as evidenced by its powerful anti-inflammatory effects in multiple *in vitro* and *in vivo* models.[22–26] This peptide does not activate CXCR3, but is a potent GAG binder and competes with inflammatory chemokines for binding to GAGs.

The current study was designed to expose the putative anti-fibrotic effects of CXCL9(74–103). Collectively, the presented data revealed for the first time that CXCL9(74–103) reduces the production of pro-fibrotic markers *in vitro* in human fibroblasts and *in vivo* in the UUO model of renal fibrosis. Fibroblast migration, which contributes to fibroblast accumulation during the fibrotic process, was suppressed in the presence of CXCL9(74–103). TGF-β, which is produced by immune and non-immune cells, is a critical pathological cytokine in renal fibrosis and CKD.
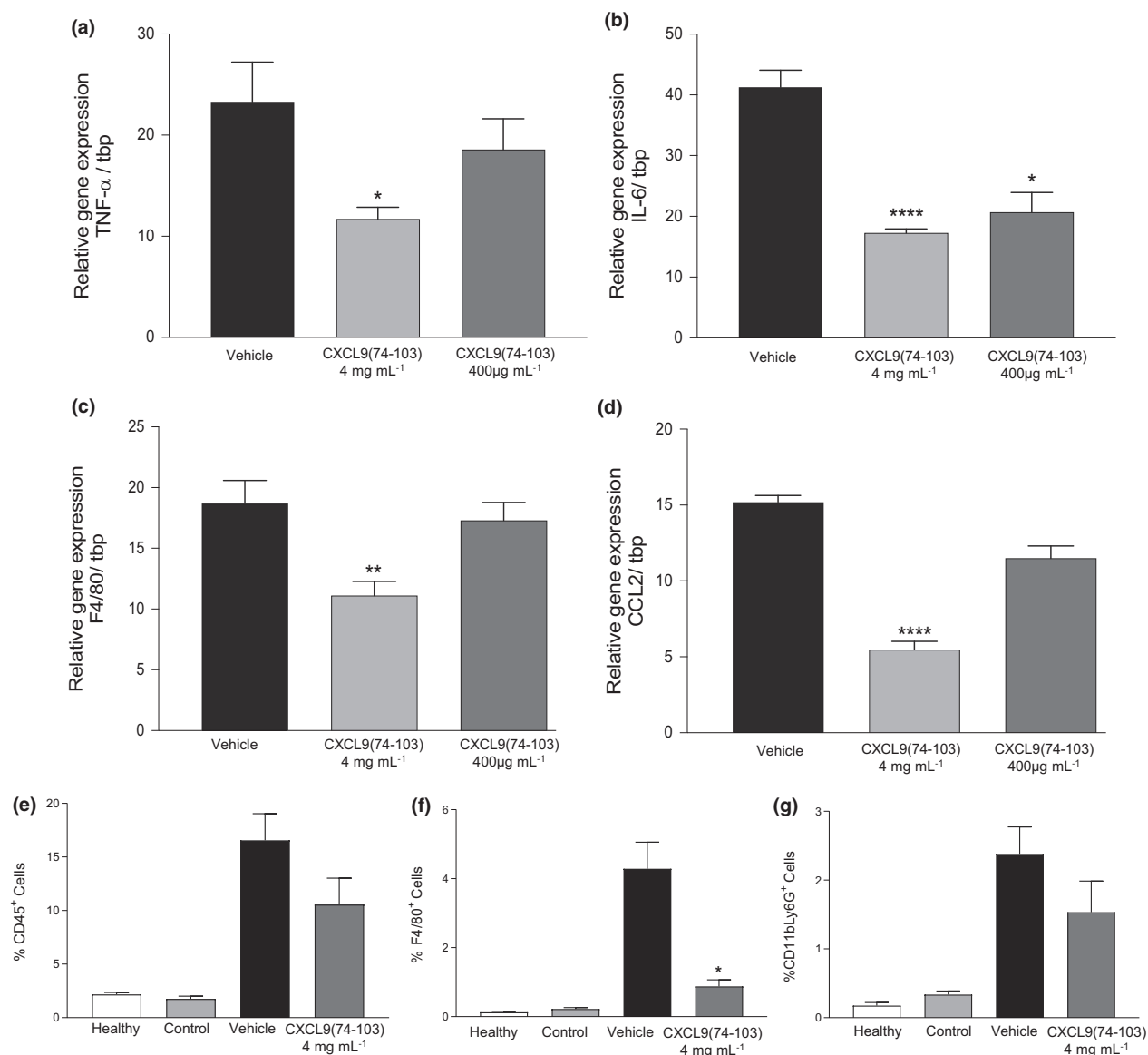
Figure 9. Effect of CXCL9(74–103) on inflammation in UUO mice. The relative gene expression levels (each cDNA sample was analysed in duplicate) of the inflammatory markers **(a)** TNF-α, **(b)** IL-6, **(c)** F4/80 and **(d)** CCL2 were evaluated in UUO kidneys treated with vehicle (PBS), 0.4 mg mL^{-1} or 4 mg mL^{-1} CXCL9(74–103) (100 µL per pump) (7 days post-surgery). The presence of **(e)** CD45$^+$, **(f)** F4/80$^+$ and **(g)** CD11b$^+$/Ly6G$^+$ leucocytes was detected by flow cytometry. Data are presented as mean ± SEM of six mice per group. *$P < 0.05$, **$P < 0.01$, ****$P < 0.001$ versus vehicle.

TGF-β signalling stimulates the conversion of resident fibroblasts to myofibroblasts, which then produce excessive amounts of extracellular matrix molecules.[29,30,49] We found that CXCL9(74–103) reduced TGF-β1-induced fibroblast activation and CTGF protein production, as well as TGF-β1-GAG interaction. The numbers of inflammatory cells and the levels of inflammatory chemokines and cytokines have been shown to increase after UUO-promoting fibrogenesis.[50] CXCL9(74–103) treatment had an inhibitory effect on the mRNA expression of TNF-α, IL-6, CCL2 and macrophage infiltration. In addition, the pro-fibrotic role of MMP-9 through stimulation of EMT has been well established in renal fibrosis. MMP-9 is capable of disrupting E-cadherin/β-catenin-mediated cell-to-cell adhesion. Besides the induction of EMT, MMP-9 cleaves the macrophage chemoattractant
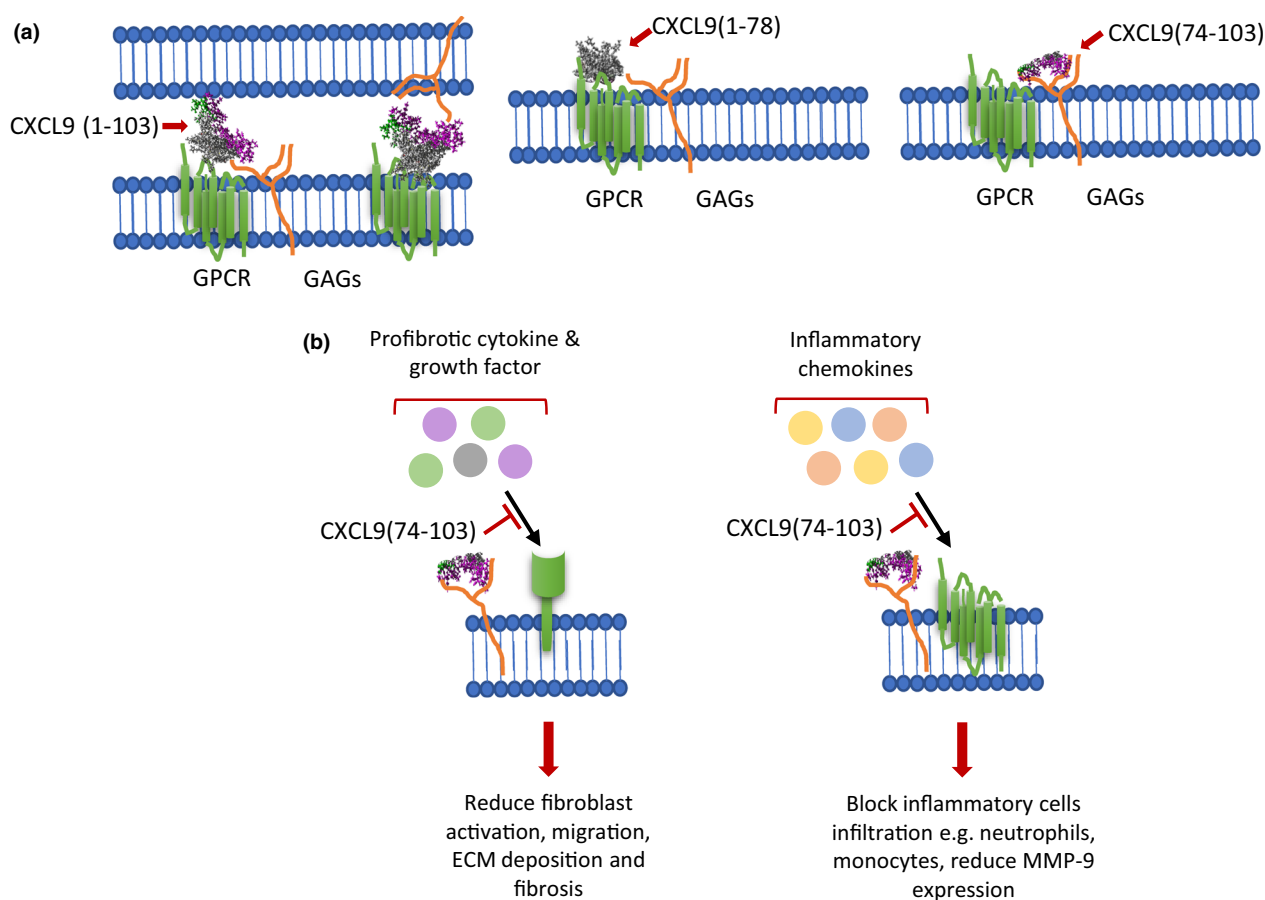
Figure 10. Schematic diagram of the mechanisms that contribute to the anti-fibrotic effect of CXCL9(74–103). **(a)** The intact CXCL9(1–103) protein is presented to its G protein-coupled receptor (GPCR) CXCR3 via GAGs present either on the target cell itself or on a nearby cell. In contrast, CXCL9(1–78) misses the positively charged COOH-terminus and can still activate CXCR3, but will be washed away quickly by the bloodstream as it cannot be anchored to the endothelial cell layer. The synthetic COOH-terminal peptide of CXCL9, CXCL9(74–103), however, has a high affinity for GAGs, but cannot activate the GPCR CXCR3. It can displace intact chemokine from the GAGs, forcing detachment of the intact chemokine from the cell membrane, thereby hampering its inflammatory activity [anti-inflammatory effect of CXCL9(74–103) in **b**]. **(b)** Schematic representation of the mechanisms behind the anti-fibrotic CXCL9(74–103). The anti-fibrotic effect of CXCL9(74–103) is dual: first by decreasing the influx of leucocytes that locally release pro-fibrotic factors; and second by competition for GAG binding with pro-fibrotic factors, for example, TGF-β. By preventing GAG binding of the pro-fibrotic factor, the latter can less efficiently activate its cognate receptor.

osteopontin (OPN).[51–54] Our peptide attenuated the protein expression of the EMT marker vimentin and mRNA expression of MMP-9, macrophage marker F4/80 and monocyte attractant CCL2. Therefore, we speculate that the CXCL9(74–103)-attenuated MMP-9 expression and the subsequent impairment of EMT and monocyte attraction may at least partially explain the beneficial effects of the CXCL9(74–103) peptide.

Cytokine secretion is one of the key mechanisms by which injured renal tubular epithelial cells promote kidney fibrogenesis.[55–57] Additionally, an increased number of myofibroblasts are associated with a lack of renal epithelial cell unity and renal tissue deformity.[53] Importantly, application of the GAG-binding peptide largely preserved renal tubular morphology, most probably because of its negative effects on EMT or myofibroblast activation/function. The suggested molecular mechanisms (schematically summarised in Figure 10) by which CXCL9(74–103) attenuates fibrosis and inflammation would be (1) by disruption of pro-fibrotic cytokine pathways, for example TGF-β-GAG interaction, which potentiates TGF-β signalling and prevents its proteolytic degradation,[30–33] and (2) by inhibition of leucocyte recruitment through competition with active chemokines for binding to GAGs.

A major challenge that faces the development of therapeutic compounds is the occurrence of adverse effects. We therefore checked the peptide's cytotoxic potential *in vitro*. Our results showed that fibroblasts remain fully viable after exposure to CXCL9(74–103). Considering the long-term treatment of chronic diseases, we anticipate that the short half-life of the peptide may be problematic. Indeed, intravenously injected CXCL9 (74–103) is rapidly (within minutes) cleared from the circulation.[22] However, peptides were retained on the endothelium much longer, indicating that cellular GAG interactions stabilise the peptide and prevent degradation. To avoid repeated intravenous injections, we used subcutaneously implanted osmotic pumps that gradually released the peptide and showed that this approach allowed treatment for multiple days. Obviously, robust research is necessary to improve the half-life of the peptide and to unravel its pharmacokinetic profile.

In summary, the present study provides relevance for interfering with chemokine–GAG and/or growth factor–GAG interactions to attenuate fibrosis. Making use of a CXCL9-derived GAG-binding peptide that is unable to activate CXCR3, we propose a novel approach to tackle fibrosis. Although follow-up research is essential, our data provide a promising strategy for the development of anti-fibrotic drugs.

METHODS

Chemical synthesis of the human CXCL9-derived peptides

The NH$_2$-terminal chemokine domain of human CXCL9, that is CXCL9(1–78), and the COOH-terminal CXCL9-derived peptide, CXCL9(74–103), were chemically synthesised based on Fmoc [*N*-(9-fluorenyl)methoxycarbonyl] chemistry using an Activo-P11 automated solid-phase peptide synthesiser (Activotec; Cambridge, UK), as described by Loos *et al.*[21] Part of the synthetic CXCL9(74–103) peptide was either site-specifically biotinylated or fluorescently labelled at the NH$_2$-terminus using biotin-*p*-nitrophenyl ester (Novabiochem, Darmstadt, Germany) or 5(6)-carboxytetramethylrhodamine (TAMRA; Merck Millipore, Darmstadt, Germany).[26] Synthetic peptides were purified on a Proto 300 C18 5-μm RP-HPLC column (10 × 150 mm; Higgins Analytical, Mountain View, CA, USA) and eluted with an acetonitrile gradient in 0.1% (v/v) trifluoroacetic acid (TFA). A portion (0.2%) of the column effluent was directly injected into an electrospray–ion trap mass spectrometer (Amazon SL ion trap, Bruker, Bremen, Germany). Fractions containing homogeneous CXCL9-derived peptide were pooled, lyophilised and dissolved in PBS. The CXCL9(1–78) protein was folded into its correct configuration as described previously.[28,58] The

purified peptides were weighed to determine the exact amount, and purity was determined by SDS-PAGE, NH$_2$-terminal protein sequencing based on Edman degradation and mass spectrometry.[21]

Cells

Human diploid fibroblasts (E$_1$SM/E$_6$SM)[59] were grown in Minimum Essential Medium (MEM) Rega-3 (Gibco/Thermo Fisher Scientific, Waltham, MA, USA) supplemented with 10% (v/v) foetal bovine serum and sodium bicarbonate. Diploid human fibroblasts were used from passage 21 to passage 30 and verified for mycoplasm contamination. Chinese hamster ovary (CHO) cells, stably transfected with human CXCR3A (CHO/CXCR3A), were kindly provided by Professor Dr M Parmentier (ULB, Brussels, Belgium) and cultured as described.[60]

Calcium signal transduction assay

The capacity of the CXCL9(1–78) peptide to induce calcium signalling through CXCR3A was tested using CXCR3A-transfected CHO cells, as previously described.[22]

Cell viability assay

Cell viability was measured using an alamarBlue assay (Thermo Fisher Scientific). Diploid fibroblasts were plated in a 96-well plate (10^4 cells per well) and subsequently incubated with CXCL9(74–103) with or without 5 ng mL^{-1} TGF-β1 (Peprotech, Rocky Hill, NJ, USA). After 48 h, the medium was removed and replaced by culture medium containing 10% (v/v) alamarBlue. Afterwards, the plates were incubated for 4 h at 37°C, and the absorbance of the reduced indicator was measured at 570 nm using a plate reader (CLARIOstar; BMG Labtech, De Meern, the Netherlands). The magnitude of alamarBlue reduction is an indicator of cell viability. Four independent experiments were performed, wherein each experimental condition was tested in duplicate.

GAG-binding assay

The ability of the CXCL9-derived peptides to compete with the pro-fibrotic cytokine TGF-β1 for GAG binding was evaluated using GAG-binding 96-well plates (Galen Laboratory Supplies, Middletown, CT, USA), which adsorb GAGs without affecting their protein-binding characteristics. HS (Iduron, Cheshire, UK) was diluted to 25 μg mL^{-1} in standard assay buffer (100 mM NaCl, 50 mM sodium acetate, 0.2% (v/v) Tween-20, and pH 7.2) and immobilised on the plasma-polymerised surface of GAG-binding plates through overnight incubation in the dark at room temperature. After three washing steps with standard assay buffer, the plates were blocked with blocking buffer (standard assay buffer enriched with 0.2% (w/v) gelatin) for 1 h at 37°C. Blocking buffer was discarded, and serial dilutions of CXCL9-derived peptide combined with recombinant human TGF-β1 were added in duplicate, followed by incubation for 2 h at 37°C. Unbound peptides and cytokines were removed by three

washes with standard assay buffer. Bound TGF-β1 was detected with biotinylated polyclonal rabbit anti-human TGF-β1 (Cat. No. BAF240; R&D Systems, Minneapolis, MN, USA), diluted in blocking buffer. After washing, horseradish peroxidase-labelled streptavidin was added, and the peroxidase activity was quantified by adding a horseradish peroxidase substrate solution. Conversion of 3,3′,5,5′-tetramethylbenzidine in the presence of 0.015% (v/v) H_2O_2 was measured at 450 nm using a Power Wave XS Microplate Spectrophotometer (BioTek, Winooski, VT, USA). The experiment was performed twice. Results represent percentages of inhibition of cytokine binding to HS.

xCELLigence migration assay

To evaluate the effect of PDGF on the migration of human diploid fibroblasts, a real-time cell analyser (xCELLigence RTCA DP System; ACEA Biosciences, San Diego, CA, USA) was employed. First, 160 μL MEM Rega-3 medium supplemented with 0.4% (v/v) foetal bovine serum (control medium) with or without 30 ng mL^{-1} PDGF-BB (Peprotech) was added to the wells of the lower chamber of a Cell Invasion and Migration (CIM)-Plate (ACEA Biosciences). After assembly of the lower and upper chamber, wells in the upper part of the chamber were filled with 50 μL of serum-free MEM Rega-3 medium with or without 0.3 or 3 μM CXCL9(74–103). After equilibration of the plate at 37°C for 1 h, cells (4 × 10^4 cells in 100 μL per well) were added. During an additional 30-min incubation period at room temperature, cells were allowed to settle onto the membrane. After transfer of the plate to the instrument, cell migration, recorded as changes in electrical impedance, was monitored every 5 min for 24 h. These values were converted into cell indices as a measure of migration. Three independent experiments were performed, with each experimental condition tested at least in duplicate within one experiment.

Induction assays

The anti-fibrotic effect of CXCL9-derived peptides was assessed *in vitro* on human fibroblast cultures. Briefly, 7.5 × 10^4 cells per well were seeded in six-well culture plates (TPP, Trasadingen, Switzerland) and grown to reach 70% confluence. Next, fibroblasts were incubated in duplicate with authentic CXCL9(1–103) (Peprotech) or CXCL9(74–103), in the presence or absence of 5 ng mL^{-1} human recombinant TGF-β1 (Peprotech). As a control, cells were cultured in medium alone. Following incubation for 48 h, cells were lysed with RLT buffer (Qiagen, Hilden, Germany) containing 1% (v/v) 2-mercaptoethanol. RNA was extracted using the RNeasy Mini Kit (Qiagen) according to the manufacturer's instructions, and converted to cDNA and used for quantitative analysis by real-time PCR analysis (see below). Four independent induction experiments were performed, and every condition was included in duplicate in each experiment. Cell culture supernatants were analysed for the presence of CTGF using a commercially available enzyme-linked immunosorbent sandwich assay (Cat. No. DY9190-05; R&D Systems), according to the manufacturers' instructions. Five independent induction experiments were performed, and each condition was included in duplicate in each experiment.

Experimental animals and surgical procedures

Male C57BL/6 mice (12 weeks old; weight of 28–30 g) were obtained from Charles River (Wilmington, MA, USA) and were housed in cages with free access to food and water. The surgical procedures started by opening of the abdomen with a midline incision under general anaesthesia (isoflurane/O$_2$). Mice were subjected to UUO by a double ligation of the left ureter proximal to the kidney using 6-0 silk sutures. Right kidneys were used as controls and were manipulated, but not ligated. Because of the limited half-life of the peptide in circulation after bolus injection, the CXCL9(74–103) peptide (0.04 or 0.4 mg in total) was delivered continuously during 7 days by osmotic pumps with a reservoir of 100 μL and flow rate of 0.5 μL h^{-1} (model 1007D; ALZET, Cupertino, CA, USA) that were implanted subcutaneously following the operation. Follow-up time was 7 days for all experiments, with the exception of the biodistribution experiments that are described below. Groups consisted of 4–6 mice per time point per read-out (measurement of fluorescence intensity, gene expression analysis, IHC or flow cytometry). All experiments involving animals were approved by the Local Animal Ethics Committee of the University of Leuven (study P045/2017).

In vivo biodistribution of TAMRA-labelled CXCL9(74–103)

At fixed time points (7 or 10 days) after surgery, mice were euthanized after anaesthesia. Blood was collected using heparin-coated Pasteur pipettes. Mice were perfused with 20 mL of phosphate-buffered saline (PBS) in order to reduce the blood content in the collected organs. Organs were collected, weighed and subsequently homogenised by a Precellys tissue homogeniser (Bertin Instruments, Montigny-le-Bretonneux, France) in 500 μL radioimmunoprecipitation (RIPA) lysis buffer (Amresco/VWR Life Science, Haasrode, Belgium) with 2.8-mm zirconium oxide beads (Bertin Instruments). Then, 50 μL of each homogenised sample was added to a black 96-well plate, and fluorescence intensity was measured using a CLARIOstar plate reader. A standard curve (in duplicate) was made with TAMRA-labelled CXCL9(74–103).

Quantitative real-time PCR

Total RNA from cells and kidney tissues was extracted using the RNeasy Mini Kit (Qiagen), according to the manufacturers' instructions. The RNA concentrations were measured on a NanoDrop ND-1000 Spectrophotometer (Isogen Life Science, Utrecht, the Netherlands). Total RNA was reverse-transcribed using the high-capacity cDNA reverse transcription kit (Applied Biosystems, Foster City, CA, USA). Subsequently, quantitative polymerase chain reactions (qPCRs) were performed using predesigned Prime Time qPCR Probe Assays from Integrated DNA Technologies (IDT, Leuven, Belgium). Expression levels of α-SMA (Hs.PT.53a.2559807, Mm.PT.58.16320644), TGF-β1 (Mm.PT.58.11254750), fibronectin (Mm.PT.58.8135568), vimentin

(Mm.PT.58.16320644), collagen III (Hs.PT.584249241, Mm.PT.58.13848686), MMP-9 (Mm.PT.58.10100097), IL-6 (Mm.PT.58.10005566), tumor necrosis factor (TNF)-α (Mm.PT.58.12575861), F4/80 (Mm.PT. 58.32717794) and the chemokine CCL2 (Mm.PT.58.422151692) were normalised to the expression of TATA box-binding protein (tbp) or 18S ribosomal RNA. All measurements were performed in duplicate.

Immunostaining

The *in vitro* anti-fibrotic effect of the CXCL9-derived peptide was checked on human diploid fibroblasts. These primary cells were grown overnight on coverslips at 37°C and 5% CO_2. Cells were incubated with CXCL9(74–103) peptide in the presence or absence of TGF-β1. After 48 h, cells were fixed with acetone/methanol (ratio 1:1) and were incubated with antibodies against α-SMA (Cat. No. 61001; ProGen, Heidelberg, Germany) and collagen III (Cat. No. ab7778; Abcam, Cambridge, UK). Visualisation of α-SMA and collagen III was realised using FITC-labelled goat anti-mouse IgG2a (Cat. No. 1081-02; Southern Biotech, Birmingham, AL, USA) and Alexa Fluor 647-labelled goat anti-rabbit (Cat. No. A21246; Invitrogen, Eugene, OR, USA) secondary antibodies, respectively.

Changes in kidney histology following UUO were analysed by periodic acid–Schiff staining (PAS) on 2-μm paraffin sections. To examine a potential anti-fibrotic role of CXCL9 (74–103) in kidney tissues, we performed α-SMA and vimentin double immunofluorescent labelling, using primary antibodies targeting α-SMA (Cat. No. 61001; ProGen) and vimentin (Cat. No. ab92547; Abcam). To study the effect of CXCL9(74–103) on extracellular matrix deposition, kidney tissues were immunohistochemically stained for fibronectin (Cat. No. ab2413; Abcam) and collagen III (Cat. No. ab7778; Abcam). Briefly, 4-μm acetone-fixed frozen sections were blocked for endogenous peroxidase activity with 3% (v/v) H_2O_2 (in PBS) followed by incubation with primary antibodies. The binding of primary antibodies was detected as described above for immunocytochemistry. We used Hoechst for nuclear counterstaining, and sections were coverslipped with ProLong Gold antifade reagent (Invitrogen). Images were acquired with a Zeiss Axiovert 200M inverted microscope and AxioVision acquisition software (Carl Zeiss, Oberkochen, Germany).

Quantification of immunostaining

To determine the *in vitro* anti-fibrotic effect of CXCL9(74–103), α-SMA and collagen III expression (number of positive pixels) was quantified in five images/coverslip (at 200× magnification starting at the centre and then above, below, right and left of the centre) using ImageJ software (ImageJ 1.46r, US National Institutes of Health, Bethesda, Maryland, USA).

The kidney sections were scanned using a Nikon NiE microscope + Marzhauser SlideExpress 2 (Nikon Instruments, Tokyo, Japan). The abundance of cortico-interstitial α-SMA, vimentin, fibronectin and collagen III (number of positive pixels) was determined using ImageJ software (ImageJ 1.46r) at 200× magnification. To assess renal tubular atrophy, PAS-stained sections were evaluated in 5 independent, randomly selected fields for each kidney. Tubular dilation was

measured by dividing the surface area of the tubular lumen by the surface area of the tubular lumen + epithelium for all individual tubules, with the use of ImageJ software. For each kidney, the mean ratio was calculated, and an increased ratio indicated tubular dilation.

Flow cytometry

Single-cell suspensions prepared from excised kidneys (200 000 cells per tube) were incubated with FcR-blocking reagent (Miltenyi Biotec, Bergisch Gladbach, Germany) and stained with the following monoclonal antibodies against mouse leucocyte markers: BUV395-conjugated anti-Ly6G, BV421-conjugated CD11b, APC-conjugated CD45, PE-Cy7-conjugated CD3 and PE-conjugated F4/80 (eBioscience, San Diego, CA, USA or BD Biosciences, East Rutherford, NJ, USA). Dead cells were excluded using Zombie Aqua 516 (BioLegend, San Diego, CA, USA). Flow cytometry was performed on a BD LSR Fortessa X20. Results were analysed using FlowJo v10 software (LLC/BD Biosciences).

Statistical analysis

Statistical analyses were performed using GraphPad Prism 5.0 software (La Jolla, CA, USA). All *in vitro* experiments were repeated at least three times, and the results represent mean ± standard error of the mean (SEM). Non-parametric statistical tests were used for non-normally distributed data. First, non-parametric one-way ANOVA (the Kruskal–Wallis test) and afterwards pairwise comparisons (Mann–Whitney U-test) were performed to detect statistical differences between the two treatment groups. A P-value < 0.05 was considered statistically significant.

CONFLICT OF INTEREST

The authors declare no conflict of interest.

AUTHOR CONTRIBUTIONS

Fariba Poosti: Conceptualization; Data curation; Formal analysis; Funding acquisition; Investigation; Methodology; Project administration; Resources; Software; Supervision;

Validation; Visualization; Writing – original draft; Writing – review & editing. **Mohammad Ayodhia Soebadi:** Methodology; Visualization; Writing – review & editing. **Helena Crijns:** Methodology; Writing – review & editing. **Alexandra De Zutter:** Methodology; Writing – review & editing. **Mieke Metzemaekers:** Methodology; Writing – review & editing. **Nele Berghmans:** Methodology; Writing – review & editing. **Vincent Vanheule:** Methodology; Writing – review & editing. **Maarten Albersen:** Funding acquisition; Resources; Writing – review & editing. **Ghislain Opdenakker:** Data curation; Formal analysis; Supervision; Writing – review & editing. **Jo Van Damme:** Data curation; Formal analysis; Funding acquisition; Supervision; Writing – review & editing. **Ben Sprangers:** Data curation; Formal analysis; Writing – review & editing. **Paul Proost:** Investigation; Supervision; Writing – original draft; Writing – review & editing. **Sofie Struyf:** Data curation; Formal analysis; Funding acquisition; Investigation; Supervision; Writing – review & editing.

REFERENCES

1. Liu Y. Renal fibrosis: new insights into the pathogenesis and therapeutics. *Kidney Int* 2006; **69**: 213–217.
2. Lee SB, Kalluri R. Mechanistic connection between inflammation and fibrosis. *Kidney Int Suppl* 2010; **119**: S22–S26.
3. Mack M. Inflammation and fibrosis. *Matrix Biol* 2018; **68–69**: 106–121.
4. Roy I, Evans DB, Dwinell MB. Chemokines and chemokine receptors: update on utility and challenges for the clinician. *Surgery* 2014; **155**: 961–973.
5. Zlotnik A, Yoshie O. Chemokines: a new classification system and their role in immunity. *Immunity* 2000; **12**: 121–127.
6. Rot A, von Andrian UH. Chemokines in innate and adaptive host defense: basic chemokinese grammar for immune cells. *Annu Rev Immunol* 2004; **22**: 891–928.
7. Bachelerie F, Ben-Baruch A, Burkhardt AM *et al*. International union of basic and clinical pharmacology. LXXXIX. Update on the extended family of chemokine receptors and introducing a new nomenclature for atypical chemokine receptors. *Pharmacol Rev* 2014; **66**: 1–79.
8. Händel TM, Johnson Z, Crown SE, Lau EK, Proudfoot AE. Regulation of protein function by glycosaminoglycans–as exemplified by chemokines. *Annu Rev Biochem* 2005; **74**: 385–410.
9. Johnson Z, Proudfoot AE, Händel TM. Interaction of chemokines and glycosaminoglycans: a new twist in the regulation of chemokine function with opportunities for therapeutic intervention. *Cytokine Growth Factor Rev* 2005; **16**: 625–636.
10. Mortier A, Van Damme J, Proost P. Overview of the mechanisms regulating chemokine activity and availability. *Immunol Lett* 2012; **145**: 2–9.
11. Weiskirchen R, Weiskirchen S, Tacke F. Organ and tissue fibrosis: molecular signals, cellular mechanisms and translational implications. *Mol Aspects Med* 2019; **65**: 2–15.
12. Sahin H, Wasmuth HE. Chemokines in tissue fibrosis. *Biochim Biophys Acta* 2013; **1832**: 1041–1048.
13. Farber JM. HuMig: a new human member of the chemokine family of cytokines. *Biochem Biophys Res Commun* 1993; **192**: 223–230.
14. Metzemaekers M, Vanheule V, Janssens R, Struyf S, Proost P. Overview of the mechanisms that may contribute to the non-redundant activities of interferon-inducible CXC chemokine receptor 3 ligands. *Front Immunol* 2018; **8**: 1970.
15. Van Raemdonck K, Van den Steen PE, Liekens S, Van Damme J, Struyf S. CXCR3 ligands in disease and therapy. *Cytokine Growth Factor Rev* 2015; **26**: 311–327.
16. Sahin H, Borkham-Kamphorst E, Kuppe C *et al*. Chemokine CXCL9 attenuates liver fibrosis-associated angiogenesis in mice. *Hepatology* 2012; **55**: 1610–1619.
17. O'Beirne SL, Walsh SM, Fabre A *et al*. CXCL9 Regulates TGF-β1-induced epithelial to mesenchymal transition in human alveolar epithelial cells. *J Immunol* 2015; **195**: 2788–2796.
18. Jiang D, Liang J, Campanella GS *et al*. Inhibition of pulmonary fibrosis in mice by CXCL10 requires glycosaminoglycan binding and syndecan-4. *J Clin Invest* 2010; **120**: 2049–2057.
19. Jiménez-Sousa MÁ, Gómez-Moreno AZ, Pineda-Tenor D *et al*. CXCL9-11 polymorphisms are associated with liver fibrosis in patients with chronic hepatitis C: a cross-sectional study. *Clin Transl Med* 2017; **6**: 26.
20. Jiang D, Liang J, Hodge J *et al*. Regulation of pulmonary fibrosis by chemokine receptor CXCR3. *J Clin Invest* 2004; **114**: 291–299.
21. Loos T, Mortier A, Proost P. Isolation, identification, and production of posttranslationally modified chemokines. *Methods Enzymol* 2009; **461**: 3–29.
22. Vanheule V, Janssens R, Boff D *et al*. The positively charged COOH-terminal glycosaminoglycan-binding CXCL9(74–103) peptide inhibits CXCL8-induced neutrophil extravasation and monosodium urate crystal-induced gout in mice. *J Biol Chem* 2015; **290**: 21292–21304.
23. Vanheule V, Boff D, Mortier A *et al*. CXCL9-derived peptides differentially inhibit neutrophil migration *in vivo* through interference with glycosaminoglycan interactions. *Front Immunol* 2017; **8**: 530.
24. Vanheule V, Crijns H, Poosti F *et al*. Anti-inflammatory effects of the GAG-binding CXCL9(74–103) peptide in dinitrofluorobenzene-induced contact hypersensitivity in mice. *Clin Exp Allergy* 2018; **48**: 1333–1344.
25. Boff D, Crijns H, Janssens R *et al*. The chemokine fragment CXCL9(74–103) diminishes neutrophil recruitment and joint inflammation in antigen-induced arthritis. *J Leukoc Biol* 2018; **104**: 413–422.
26. Vanheule V, Vervaeke P, Mortier A *et al*. Basic chemokine-derived glycosaminoglycan binding peptides exert antiviral properties against dengue virus serotype 2, herpes simplex virus-1 and respiratory syncytial virus. *Biochem Pharmacol* 2016; **100**: 73–85.
27. Wasmuth HE, Lammert F, Zaldivar MM *et al*. Antifibrotic effects of CXCL9 and its receptor CXCR3 in livers of mice and humans. *Gastroenterology* 2009; **137**: 309–339.
28. Metzemaekers M, Mortier A, Janssens R *et al*. Glycosaminoglycans regulate CXCR3 ligands at distinct levels: protection against processing by dipeptidyl peptidase IV/CD26 and interference with receptor signaling. *Int J Mol Sci* 2017; **18**: 1513.
29. Schnaper HW, Jandeska S, Runyan CE *et al*. TGF-β signal transduction in chronic kidney disease. *Front Biosci* 2009; **14**: 2448–2465.

30. Tomasek JJ, Gabbiani G, Hinz B, Chaponnier C, Brown RA. Myofibroblasts and mechano-regulation of connective tissue remodelling. *Nat Rev Mol Cell Biol* 2002; **3**: 349–363.

31. Choi SH, Lee JY, Suh JS, Park YS, Chung CP, Park YJ. Dual-function synthetic peptide derived from BMP4 for highly efficient tumor targeting and antiangiogenesis. *Int J Nanomedicine* 2016; **11**: 4643–4656.

32. Lyon M, Rushton G, Gallagher JT. The interaction of the transforming growth factor-βs with heparin/heparan sulphate is isoform-specific. *J Biol Chem* 1997; **272**: 18000–18006.

33. McCaffrey TA, Falcone DJ, Du B. Transforming growth factor-β1 is a heparin-binding protein: identification of putative heparin-binding regions and isolation of heparins with varying affinity for TGF-β1. *J Cell Physiol* 1992; **152**: 430–440.

34. Koehler L, Samsonov S, Rother S *et al.* Sulfated hyaluronan derivatives modulate TGF-β1: receptor complex formation: possible consequences for TGF-β1 signaling. *Sci Rep* 2017; **7**: 1210.

35. Klinkhammer BM, Floege J, Boor P. PDGF in organ fibrosis. *Mol Aspects Med* 2018; **62**: 44–62.

36. Tsai CC, Wu SB, Kau HC, Wei Y. Essential role of connective tissue growth factor (CTGF) in transforming growth factor-β1 (TGF-β1)-induced myofibroblast transdifferentiation from Graves' orbital fibroblasts. *Sci Rep* 2018; **8**: 7276.

37. Kobayashi T, Kim H, Liu X *et al.* Matrix metalloproteinase-9 activates TGF-β and stimulates fibroblast contraction of collagen gels. *Am J Physiol Lung Cell Mol Physiol* 2014; **306**: L1006–L1015.

38. Yu Q, Stamenkovic I. Cell surface-localized matrix metalloproteinase-9 proteolytically activates TGF-β and promotes tumor invasion and angiogenesis. *Genes Dev* 2000; **14**: 163–176.

39. Lira SA, Furtado GC. The biology of chemokines and their receptors. *Immunol Res* 2012; **54**: 111–120.

40. Nagarsheth N, Wicha MS, Zou W. Chemokines in the cancer microenvironment and their relevance in cancer immunotherapy. *Nat Rev Immunol* 2017; **17**: 559–572.

41. Ding J, Tredget EE. The role of chemokines in fibrotic wound healing. *Adv Wound Care (New Rochelle)* 2015; **4**: 673–686.

42. Eming SA, Wynn TA, Martin P. Inflammation and metabolism in tissue repair and regeneration. *Science* 2017; **356**: 1026–1030.

43. Hillebrandt S, Goos C, Matern S, Lammert F. Genome-wide analysis of hepatic fibrosis in inbred mice identifies the susceptibility locus Hfib1 on chromosome 15. *Gastroenterology* 2002; **123**: 2041–2051.

44. Gerlza T, Hecher B, Jeremic D *et al.* A combinatorial approach to biophysically characterise chemokine-glycan binding affinities for drug development. *Molecules* 2014; **19**: 10618–10634.

45. Blackhall FH, Merry CL, Davies EJ, Jayson GC. Heparan sulfate proteoglycans and cancer. *Br J Cancer* 2001; **8**: 1094–1098.

46. Rek A, Krenn E, Kungl AJ. Therapeutically targeting protein-glycan interactions. *Br J Pharmacol* 2009; **157**: 686–694.

47. Trinker MU, Kungl AJ. Targeting chemokine–glycan interactions: the Cell Jammer® technology platform. *Drug Discov Today Technol* 2012; **9**: e227–e314.

48. Sadir R, Imberty A, Baleux F, Lortat-Jacob H. Heparan sulfate/heparin oligosaccharides protect stromal cell-derived factor-1 (SDF-1)/CXCL12 against proteolysis induced by CD26/dipeptidyl peptidase IV. *J Biol Chem* 2004; **279**: 43854–43860.

49. Chen L, Yang T, Lu DW *et al.* Central role of dysregulation of TGF-β/Smad in CKD progression and potential targets of its treatment. *Biomed Pharmacother* 2018; **101**: 670–681.

50. Grande MT, Pérez-Barriocanal F, López-Novoa JM. Role of inflammation in tubulo-interstitial damage associated to obstructive nephropathy. *J Inflamm (Lond)* 2010; **7**: 19.

51. Zakiyanov O, Kalousová M, Zima T, Tesař V. Matrix metalloproteinases in renal diseases: a critical appraisal. *Kidney Blood Press Res* 2019; **44**: 298–330.

52. Tan TK. Matrix metalloproteinase-9 of tubular and macrophage origin contributes to the pathogenesis of renal fibrosis via macrophage recruitment through osteopontin cleavage. *Lab Invest* 2013; **93**: 434–449.

53. Liu Y. Epithelial to mesenchymal transition in renal fibrogenesis: pathologic significance, molecular mechanism, and therapeutic intervention. *J Am Soc Nephrol* 2004; **15**: 1–12.

54. Scatena M, Liaw L, Giachelli CM. Osteopontin: a multifunctional molecule regulating chronic inflammation and vascular disease. *Arterioscler Thromb Vasc Biol* 2007; **27**: 2302–2309.

55. Friedman SL, Sheppard D, Duffield JS, Violette S. Therapy for fibrotic diseases: nearing the starting line. *Sci Transl Med* 2013; **5**: 167sr1.

56. Forbes MS, Thornhill BA, Minor JJ, Gordon KA, Galarreta CI, Chevalier RL. Fight-or-flight: murine unilateral ureteral obstruction causes extensive proximal tubular degeneration, collecting duct dilatation, and minimal fibrosis. *Am J Physiol Renal Physiol* 2012; **303**: F120–F129.

57. Lu X, Gao B, Wang Y, Liu Z, Yasui T, Liu P. Renal tubular epithelial cell injury, apoptosis and inflammation are involved in melamine-related kidney stone formation. *Urol Res* 2012; **40**: 717–723.

58. Moelants EA, Loozen G, Mortier A *et al.* Citrullination and proteolytic processing of chemokines by *Porphyromonas gingivalis*. *Infect Immun* 2014; **82**: 2511–2519.

59. Billiau A, Van Damme J, Van Leuven F *et al.* Human fibroblast interferon for clinical trials: production, partial purification, and characterisation. *Antimicrob Agents Chemother* 1979; **16**: 49–55.

60. Van Raemdonck K, Gouwy M, Lepers SA, Van Damme J, Struyf S. CXCL4L1 and CXCL4 signaling in human lymphatic and microvascular endothelial cells and activated lymphocytes: involvement of mitogen-activated protein (MAP) kinases, Src and p70S6 kinase. *Angiogenesis* 2014; **17**: 631–640.